Slip-Length Scaling in Large Earthquakes: The Role of Deep-Penetrating Slip below the Seismogenic Layer

by Bruce E. Shaw and Steven G. Wesnousky

Abstract   Coseismic slip is observed to increase with earthquake rupture length for lengths far beyond the length scale set by the seismogenic layer. The observation, when interpreted within the realm of static dislocation theory and the imposed limit that slip be confined to the seismogenic layer, implies that earthquake stress drop increases as a function of rupture length for large earthquakes and, hence, that large earthquakes differ from small earthquakes. Here, a three-dimensional elastodynamic model is applied to show that the observed increase in coseismic slip with rupture length may be satisfied while maintaining a constant stress drop across the entire spectrum of earthquake sizes when slip is allowed to penetrate below the seismogenic layer into an underlying zone characterized by velocity-strengthening behavior. Is this deep coseismic slip happening during large earthquakes? We point to a number of additional associated features of the model behavior that are potentially observable in the Earth. These include the predictions that a substantial fraction, on the order of one-third of the total coseismic moment, is due to slip below the seismogenic layer and that slip below the seismogenic layer should be characterized by long rise times and a dearth of high-frequency motion.

Introduction

Scholz (1982) pointed out many years ago the observation that average slip in large earthquakes continued to increase with rupture length well beyond the seismogenic crust depth. He noted this observation was puzzling because it was expected that ruptures broke dynamically only down to the bottom of the seismogenic depth, and this finite depth would be expected to saturate the slip for very large events if the constant stress-drop scaling for small earthquakes (Hanks, 1977) continued to hold for the large earthquakes. A debate ensued about whether the largest earthquakes continued to have even larger slip (Scholz, 1982; Pegler and Das, 1996; Henry and Das, 2001) or the slip eventually saturated (Romanowicz, 1992, 1994; Scholz, 1994; Bodin and Brune, 1996) and about whether longer length scales (Romanowicz, 1992; Scholz, 1994) or multiple length scales (Manighetti *et al.*, 2007) might be entering into the problem. This debate has important implications for earthquake hazard analysis because it is the largest events that dominate the net slip along faults, and this plays a role in determining how often the large events will occur as well as how strong the shaking will be in these events. The empirical scaling of slip versus area of rupture (a related but slightly different question from slip versus length scaling) plays a central role in current earthquake hazard estimates, and differences in assumed scaling have significant impacts on the estimates (Wells and Coppersmith, 1994; Hanks and Bakun, 2002; Working Group on California Earthquake Probabilities (WGCEP), 2003, 2007). Understanding the physical basis of the slip-length scaling would help to better understand which moment-area scalings to use and how best to extrapolate them to the largest events.

A central question arising from the observations was whether differing physical processes were needed to account for the differences between the large and small earthquakes in the empirical scaling of slip and inferred stress drop. Shaw and Scholz (2001) found that numerical simulations of scale invariant physics were able to match the observations of slip-length scaling both in terms of the mean and the scatter, suggesting that new unaccounted for physical processes were not needed. Their results reaffirmed the surprising feature of the data that the slip of the largest events continued to increase at length scales much longer than the seismogenic depth. This puzzle has led to recent attempts at an explanation, including one involving multiple length scales based on fault segmentation (Manighetti *et al.*, 2007). Building on an idea originally proposed by Das (1982), King and Wesnousky (2007) showed that the apparent conflict with static elastic dislocation theory (increase in stress drop) implied by the increase of slip with length for large earthquakes is resolved if some significant fraction of coseismic slip is allowed to extend below the base of the seismogenic layer into a medium of stable sliding that

remains stressed at or close to failure. Here, we look in more detail at the three-dimensional elastodynamic model studied by Shaw and Scholz (2001) and find that slip in the model in the largest events is indeed penetrating deep into the stably sliding lower fault. The penetration of rapid coseismic slip into the underlying zone of stable slip decreases the effective vertical stiffness and thereby allows additional slip in the seismogenic layer. Thus, we find a physical basis for the puzzling scaling seen in the numerical simulations that match well the observations, and we find that the deep slip hypothesis in the Das (1982) and King and Wesnousky (2007) explanations is indeed being chosen dynamically by a physical model. This poses a key question for earthquakes: is slip penetrating coseismically much deeper than is typically assumed in seismological, geodetic, and seismic hazard models, and how might we determine that?

The Model

The model bulk consists of a three-dimensional scalar wave equation (mode III elastic). The rectangular bulk is loaded at constant velocity on a far boundary parallel to a vertical fault. At the top and bottom of the bulk we have free boundary conditions, and in the direction along the length of the fault we use periodic boundary conditions. Close to the far loading boundary, we use a viscous layer to damp out waves and minimize reflections. On the fault we use a frictional boundary condition with the strain being equal to the frictional stress on it. The friction on the fault is the source of all the nonlinearity in the problem and is the key to all the interesting complex behavior.

Two kinds of friction are used on the fault. At depth it is stably sliding velocity-strengthening friction. Above that, in a seismogenic layer extending from the top down to the seismogenic depth, it is unstably sliding with a mixture of slip and velocity-weakening friction (Shaw and Rice, 2000; Shaw and Scholz, 2001; see the Appendix for more model details). This seismogenic depth H sets the fundamental length scale in the problem, which we scale all lengths in the problem to and thus define as unity, a length scale in the real earthquake problem corresponding to around 15 km for vertical strike-slip faults (for dipping faults, the relevant length is the down-dip fault width, so H is much wider for shallow dipping subduction zone events). When we run the model for a long time, it settles down (after a few large event cycles) onto an attracting statistically steady state. For a range of frictional weakening parameters in the problem (see the Appendix for details), we get a wide range of sizes of the large events that do not break the whole length of the fault and on which we can thus examine slip-length scaling issues. The scaling results we present in the following discussion appear to be quite insensitive to essentially all of the parameters in the problem, when we operate with large domains and are in the regime where we get a range of sizes of large events.

Results

Figure 1 shows the scaling of mean surface slip D with surface rupture length L in the model. Only events that break the surface are shown. The individual circles are for individual model events. Shaw and Scholz (2001) demonstrated the remarkable similarity of this measurement in the model as compared with earthquake data for large strike-slip events, not only in terms of the average behavior but also the scatter around the average. The solid line on this plot shows the scaling proposed by Shaw and Scholz (2001) for a constant stress-drop model that takes into account the finite width H of the seismogenic layer and the free surface at the top:

$$D \sim \begin{cases} \frac{1}{\frac{1}{L}+\frac{1}{L}} & L \le 2H, \\ \frac{1}{\frac{1}{L}+\frac{1}{2H}} & L > 2H. \end{cases} \quad (1)$$

The dashed line shows this same scaling law where we have now added a scaling factor λ to increase the seismogenic width H to have an effective mechanical width W, so now $W = \lambda H$, and H in equation (1) is replaced by λH. In the figure, we have also rescaled the amplitude, so the asymptotic slip for very large events is the same for the two curves. The solid line scaling in equation (1) with H assumes the slip extends only to the bottom of the seismogenic zone. Manighetti *et al.* (2007) allowed for a λ scaling related to rupture length to better empirically fit the observed data. Here, we consider the generalized λ scaling based on the increased penetration depth of slip, leading to a larger effective width. In Figure 1 we show a fit for a mechanical width W that is an effective tripling of H, using $\lambda = 3$. As can be seen
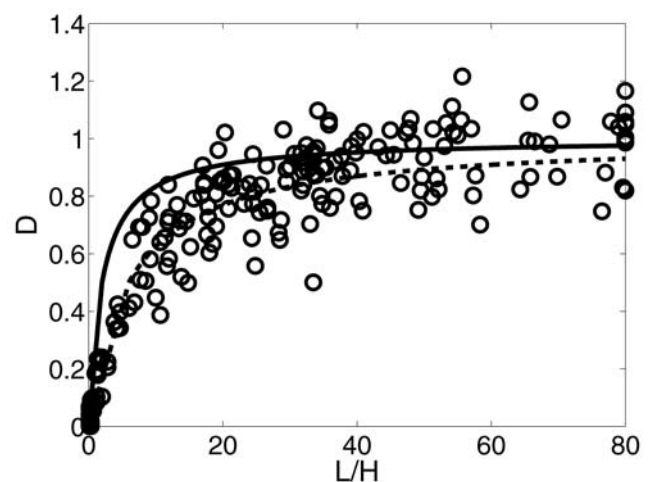

Figure 1. Average surface slip D versus rupture length L for large surface rupturing events in a three-dimensional scalar elastodynamic model. Length L is scaled by the seismogenic width H showing the aspect ratio of the ruptures. Individual circles are for individual rupture events. The solid curve is with H as in equation (1). The dashed line shows fit for larger $W = 3H$.

by eye, this rescaled W provides a much better fit to the model data. Manighetti *et al.* (2007) find the best-fitting values of $\lambda \approx 3$ for their earthquake data set; they argue, however, for multiple integer values of λ based on fault segmentation. Instead, in what follows, we show the rescaled W has a basis, at least in our numerical models, in the way the slip penetrates deeply coseismically into the stably sliding lower fault below the seismogenic zone.

Comparing Figure 1 with observations, the longest model events are much longer than the longest observed events; the largest observed aspect ratios for earthquakes, which occur in very long strike-slip events, have $L \sim 400$ km, which for $H = 15$ km gives an $L/H \sim 25$ or 30. Our largest aspect ratios of 80 here in the model are thus much longer than the longest observed events. This helps, however, to elucidate the asymptotic behavior for very long events, and it also helps to explain why saturation of slip in the observations is barely, if at all, seen: at aspect ratio 30 the model is also just barely beginning to saturate in slip.

Figure 2 illustrates the key behavior we are observing from a seismic point of view of slip penetrating coseismically quite deep. We plot a vertical array of velocity seismometers placed on the model fault, going from the surface to well below the seismogenic layer and plotting the velocities as a function of time, for an example large model event. To aid in visualizing the curves, a vertical offset proportional to the depth of the velocity meter is added. The array is located in a narrow vertical strip surrounding the epicenter of this example large event. Only nonzero velocities are shown. We see a key difference for behavior between the seismogenic upper fault, which slips with both long-period motion and lots of high frequencies, which shows in the very jagged behavior of the velocity curves as a function of time, and the stably sliding lower fault, which slips much more smoothly and with mainly long-period motion. Note also the time delay in rapid slip as the slip pushes deeper and deeper into the stably sliding layer, with the leading rupture front propagating through the seismogenic layer. Note as well, however, that this time delay is not large compared to the rupture timescale: these significant motions occurring on the stably sliding deep fault are happening coseismically. Indeed, while there is some afterslip, we are getting substantial deep coseismic slip, and it is this deep coseismic slip that is feeding back mechanically into the slip in the seismogenic layer. One other important point can be made from this plot: the deeper coseismic slip may not be easy to see in seismological inversions of fault slip, which are much more sensitive to the broad spectrum radiating seismogenic layer than the low-frequency deeper layers, but they would be a key signal to look for to image this behavior.

How significant is this lower frequency slip in the deeper layers? Figure 3 shows a plot of the ratio of the coseismic moment below the seismogenic layer to the moment in the seismogenic layer. We see that something on the order of one-half of the seismogenic moment, or one-third of the total moment, is occurring in this deeper stably sliding
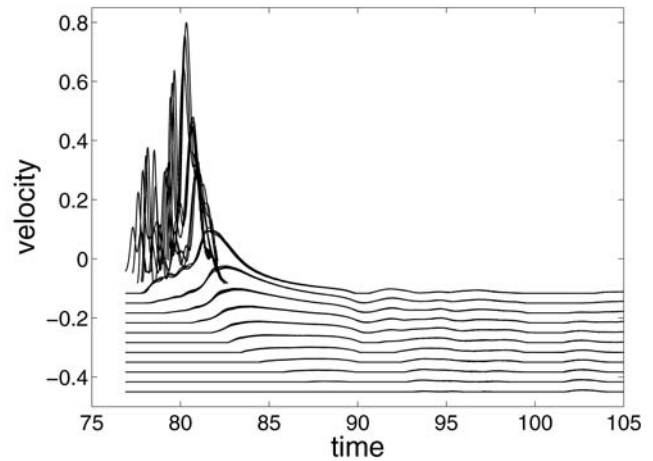

Figure 2. Velocity as a function of time for an example large event on an array of velocity meters. The array is placed along strike around the epicenter, down depth of the fault. For ease in visualization, velocity is offset proportional to depth z, with the offset equal to $0.1z/H$. At each depth five velocity meters laterally are displaced at spacing $H/6$ around the hypocenter in the along-strike direction; the width of the line gives a sense of spread in velocities along strike near the epicenter. In the depth direction, 14 of these lateral velocity meter lines are shown. Note high-frequency motions at shallow depths, in addition to the low-frequency component, while motion at depth is mainly low frequency. Only nonzero velocities are plotted. Note the delay of the onset of rapid motion at increased depths, as slip is driven deeper, but also note substantial coseismic slip on stably sliding lower fault. Units are dimensionless; for time, it is the time is takes a wave propagating at the shear-wave velocity to propagate the seismogenic crust depth H; thus, a time of unity corresponds to around 5 sec for a 3 km/sec shear wave propagating across 15 km. For velocity, the unit corresponds to the stress drop divided by the shear modulus times the shear velocity, a number around 0.3 m/sec for typical Earth values (see the appendix in Shaw [2006] for full dimensionfull conversions).
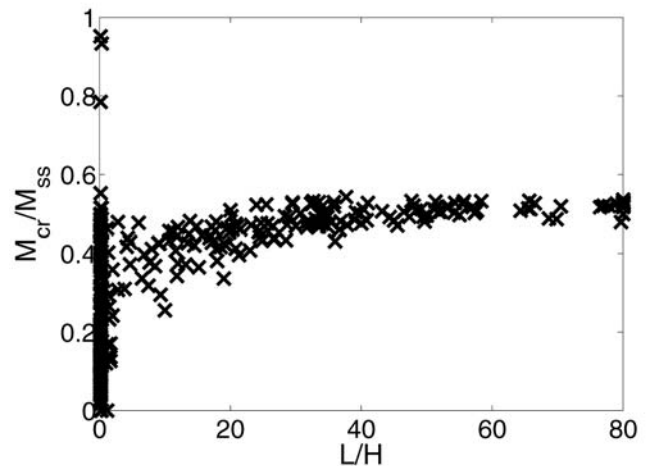

Figure 3. Moment in the stable sliding deeper layer divided by moment in the unstably sliding seismogenic layer. Values on the order of one-half of the seismogenic moment, or on the order of one-third of the total moment, are found for the very large events.
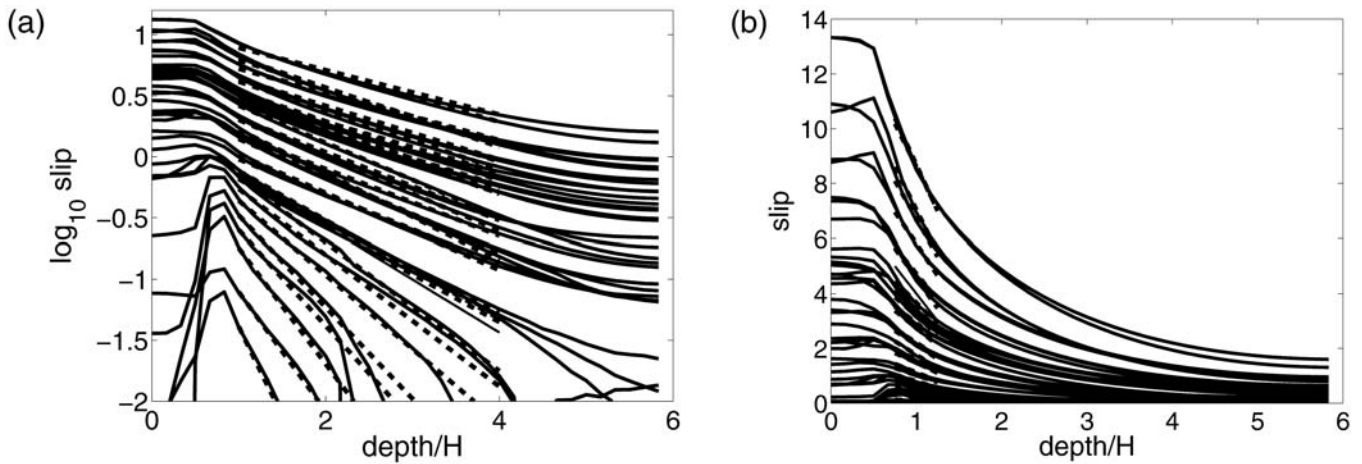
Figure 4. Slip averaged along strike as a function of depth for individual events, shown with thick solid lines. (a) Vertical axis is logarithmic scale; horizontal axis is linear scale. Thin dashed lines show exponential fit to fall-off of slip with depth below the seismogenic layer, with fit between depths H and $4H$. The thin lines show an exponential decay scale H for comparison. (b) Linear scales on vertical and horizontal axes. Thin dashed lines show linear fit to fall-off of slip with depth around the bottom of the seismogenic layer. The thin line shows a linear fall-off that has a slip that extrapolates to zero at the depth $W = 2H$.

layer (comparable fractions of the moment occur for other friction parameter values, though the exact numbers do depend somewhat on the friction parameters). This suggests one potential way of detecting this deeper slip: inversions sensitive to different frequency bands would place the low-frequency moment release at locations that differ from higher frequency motion. This approach is not without complications, however, as directivity effects can also shift centroids of different frequency bands.

A plot of the slip as a function of depth, Figure 4, gives an indication of what the deep slip looks like. Figure 4 shows for each large model event the slip averaged along strike plotted as a function of depth. The depth unity marks the

Figure 5. Depth W where slip extrapolates to zero slip from the slip-depth profile, as fit in Figure 4b, as a function of rupture length L. Note the roughly doubling of the effective width W relative to seismogenic width H for large aspect ratio L/H.

transition from the velocity-weakening seismogenic to the velocity-strengthening stably sliding lower fault. We plot the log of the slip on the vertical axis against the linear depth on the horizontal axis in Figure 4a. We see that the slip is well fit by an exponential decay into the stably sliding layer. To best describe the mechanical impact of the deep slip, we fit a linear function to the slip around the seismogenic depth, shown in Figure 4b. Extrapolating this linear fit down to the depth where the slip would be zero gives an effective width W. While these slip profiles are not simple self-similar profiles as postulated in King and Wesnousky (2007), the deep extended slip does play an analogous important mechanical role, as we will see.

Figure 5 shows these effective W length scales plotted as a function of the length of the rupture. We see a significant increase of W above H for ruptures with L longer than a few H, and some continued increase for larger L. The small continued increase of W with L plays out into a somewhat larger best-fitting single value of λ than the individual values of W might suggest: if we do a least-squares fit for the data for a best-fitting λ in Figure 1, we get $\lambda = 4.1$, which is larger than the values of W found in Figure 5. This is an effect caused by the increasing W dependence of L. This has important implications for inferring W from a best-fitting value from observational data of $\lambda \approx 3$: it does not mean that $W/H \approx 3$ necessarily in the Earth, but rather it could mean $W/H < 3$ with W increasing somewhat with L.

That these W are indeed impacting the seismogenic slip mechanically can be seen when we correct individual events based on their individual W. Figure 6 shows the estimated mean stress drops for the same model events as shown in Figure 1, where we take into account the length scales of the ruptures and compare the estimated stress drops with the average of the stress drops measured directly on the
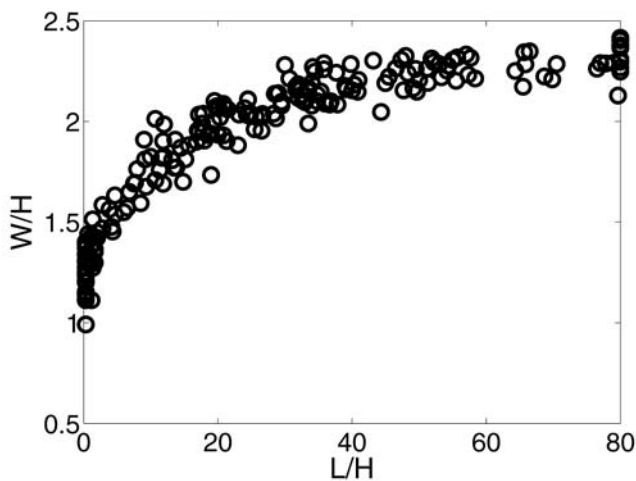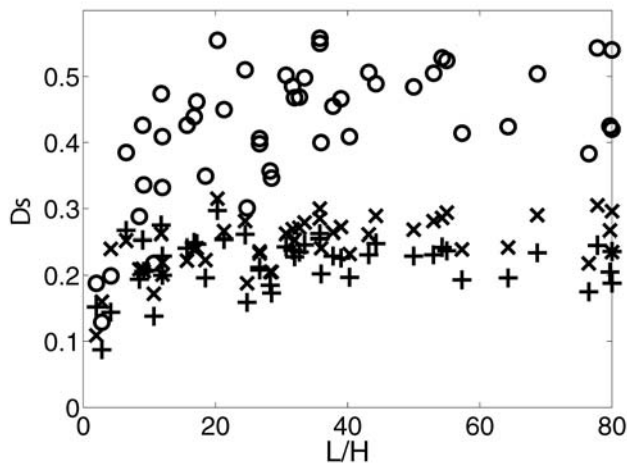
Figure 6. Average stress drop $\Delta\sigma$ versus rupture length L for events in Figure 1. Measured values of mean stress drop in events are shown with crosses (×). Estimated values when penetration depth W is taken into account are shown with pluses (+). Circles show estimates of stress drop for the same events but assuming that the depth of rupture is fixed to the depth of the seismogenic layer H. Note effective W is much better fit to measured values than H is.

seismogenic rupture areas (that is, areas within the seismogenic zone with depth $z < H$ that ruptures); these measured average stresses are shown with the cross symbol (×). To estimate the stress drops of the large events (large events are defined here as those with seismogenic rupture area $A > 2H^2$), we estimate the along-strike lengths using A/H, where A for real earthquakes would be determined from aftershock distributions. (Using A/H as an estimate for the along-strike length instead of L makes little difference for the very large events, but it is a slightly better estimate for events that barely rupture the surface.) For the width of the ruptures we examine estimates of stress drop $\Delta\sigma$ using W and H. Based on the Knopoff (1958) solution but modifying for finite A, we obtain

$$\Delta\sigma = D\left(\frac{1}{A/H} + \frac{1}{2W}\right). \qquad (2)$$

(The modulus here is dimensionless, scaled to unity.) As can be seen in Figure 6, the estimates using W, shown with the plus symbols (+), are quite good—generally within 10 or a few tens of percent, with, importantly, no bias with L. They are slightly systematically low, but this is not very important in that the prefactor depends on a very simple assumption about the slip geometry, equation (2). What is most important is that there is no systematic dependence on L. Note as well the estimates are much superior to those using H, shown with the circle symbol, with the pluses from W falling much closer to the directly measured cross values than the circle estimates using H; moreover, the circle H estimates also have an undesirable systematic error dependence on L. Note that the direct measurements of stress drop and the estimated average

values from slip and rupture lengths are completely independent, and thus, the tracking of the measurement fluctuations up and down by the estimates indicates we are capturing a key part of the process and provides additional support for the methodology.

In Figure 6 the stress drops appear nearly constant across all length scales. This is not always the case for all friction parameter values—there can, for example, be some slight increase in stress drop with increased rupture length. What is most robust, however, is that the stress drops that do occur are best tracked by W rather than H, and it is the W dependence on L along with any potential stress-drop changes that is needed to explain the slip-length scaling.

Comparison with Observations

While the prevailing view is that significant coseismic slip is mainly restricted to the seismogenic layer, with perhaps some slight penetration below that over small distances, we can ask whether the observations require this. Global Positioning System (GPS) observations generally have little depth resolution (Thatcher *et al.*, 1997), especially below the upper 5 km or so on vertical strike-slip faults even under the best circumstances (M. Page *et al.*, unpublished manuscript, 2007), and need to be in place beforehand to distinguish coseismic slip from afterslip. King and Wesnousky (2007) discuss GPS constraints in more detail and infer that deep coseismic slip is not ruled out by current observations.

Seismic inversions for slip also suffer greatly from spatial resolution problems (Beresnev, 2003). While they are relatively robust at reconstructing moment rate of the rupture, mapping this spatially onto the fault suffers from a tremendous nonuniqueness problem and is reflected in the huge variability in mapped slip of the same large ruptures from different groups (Mai, 2007), as, for example, the different inversions for the 1992 M_w 7.3 Landers earthquake (Cohee and Beroza, 1994; Wald and Heaton, 1994; Cotton and Campillo, 1995; Zeng and Anderson, 1996; Hernandez *et al.*, 1999). Many inversions do seem to prefer to add slip deeper than is often considered, evidenced by slip piling up at the bottom edges of the inversions (for example, for Landers [Wald and Heaton, 1994; Cotton and Campillo, 1995]). But this also reflects a lack of sensitivity at these depths, so one should be cautious to not overinterpret this.

When we have both seismic and GPS measurements available, while they often agree well on total moment, they also typically have substantial differences in where they ascribe slip (for example, Konca *et al.* [2007]). This illustrates well our main point about the observational constraints on potentially deep coseismic slip: we do not expect that the slip is evading detection, rather that there are insufficient constraints on where it is happening. It is not missing slip, but misplaced slip we are looking for.

Aftershocks do a remarkably good job of illuminating the rupture area in the seismogenic region. But at depths below the seismogenic zone, the stably sliding lower fault is

conditionally stable, potentially supporting ruptures into it but not initiating ruptures, and thus aftershock depths do not constrain the depth extent of slip for large events.

Figure 2 motivates a look at depth dependent differences between high-frequency mapping of fault slip and low-frequency inversions. In the case of the great M 9.1 2004 Sumatra tsunami earthquake, the high-frequency centroid (Ishii *et al.*, 2005) tends to be deeper than the moment centroid (Tsai *et al.*, 2005), likely due to extensive slip in stable sliding nonseismogenic shallower layers. Thus, while the effect we describe of differences in location between broadband and low-frequency slip appears to be occurring and measurable, the shallow stably sliding parts seem to be dominating, in terms of moment centroid, a potential contribution due to the deeper stably sliding parts.

Conclusion

We have shown in a three-dimensional elastodynamic model that significant coseismic slip can penetrate deep into the stably sliding fault below the seismogenic layer during very large events. This deeper slip occurs with little high-frequency radiation, and thus it would be easy to mislocate seismologically. It occurs despite the fact that slip in the stably sliding layer is an energy sink but as a consequence accommodates additional slip through a reduced effective vertical stiffness in the upper seismogenic layer. In the model, on the order of one-half the seismogenic moment, or one-third the total moment, occurs in the deeper stably sliding lower layer. The observed exponential fall-off of slip with depth in these model events plays a mechanical role of increasing the effective coseismic depth. This increased effective depth matches well our observed slip versus length scaling data and matches the measured stress drops in the model. The key questions now are whether this same mechanism is operating in the Earth and whether significant coseismic slip is occurring below the seismogenic layer.

Acknowledgments

References

Beresnev, I. (2003). Uncertainties in finite-fault slip inversions: to what extent to believe? (A critical review), *Bull. Seismol. Soc. Am.* **93,** 2445–2458.

Bodin, P., and J. N. Brune (1996). On the scaling of slip with rupture length for shallow strike-slip earthquakes: quasistatic models and dynamic rupture propagation, *Bull. Seismol. Soc. Am.* **86,** 1292–1299.

Cohee, B., and G. Beroza (1994). Slip distribution of the 1992 Landers earthquake and its implications for earthquake source mechanics, *Bull. Seismol. Soc. Am.* **84,** 692–712.

Cotton, F., and M. Campillo (1995). Frequency domain inversion of strong motions;application to the 1992 Landers earthquake, *J. Geophys. Res.* **100,** 3961.

Das, S. (1982). Appropriate boundary-conditions for modeling very long earthquakes and physical consequences, *Bull. Seismol. Soc. Am.* **72,** 1911–1926.

Dieterich, J. H. (1979). Modeling of rock friction, 1: Experimental results and constitutive equations, *J. Geophys. Res.* **84,** 2161.

Hanks, T. C. (1977). Earthquake stress-drops, ambient tectonic stresses, and the stresses that drive plates, *Pure Appl. Geophys.* **115,** 441–458.

Hanks, T. C., and W. H. Bakun (2002). A bilinear source-scaling model for M-log A observations of continental earthquakes, *Bull. Seismol. Soc. Am.* **92,** 1841–1846.

Henry, C., and S. Das (2001). Aftershock zones of large shallow earthquakes: fault dimensions, aftershock area expansion and scaling relations, *Geophys. J. Int.* **147,** 272.

Hernandez, B., F. Cotton, and M. Campillo (1999). Contribution of radar interferometry to a two-step inversion of the kinematic process of the 1992 Landers earthquake, *J. Geophys. Res.* **104,** 13,083.

Hillers, G., and S. G. Wesnousky (2008). Scaling relations of strike-slip earthquakes with different slip-rate-dependent properties at depth, *Bull. Seismol. Soc. Am.* **98,** 1085–1101.

Ishii, M., P. M. Shearer, H. Houston, and J. E. Vidale (2005). Extent, duration and speed of the 2004 Sumatra-Andaman earthquake imaged by the Hi-Net array, *Nature* **435,** 933–936, doi 10.1038/nature03675.

King, G. L., and S. Wesnousky (2007). Scaling of fault parameters for continental strike-slip earthquakes, *Bull. Seismol. Soc. Am.* **97,** 1833–1840, doi 10.1785/0120070048.

Knopoff, L. (1958). Energy release in earthquakes, *Geophys. J. R. Astron. Soc.* **1,** 44.

Konca, A. O. *et al.* (2007). Rupture kinematics of the 2005 M_w 8.6 Nias-Simeulue earthquake from the joint inversion of seismic and geodetic data, *Bull. Seismol. Soc. Am.* **97,** S307–S322, doi 10.1785/0120050632.

Langer, J. S., and H. Nakanishi (1993). Models of rupture propagation II: two dimensional model with dissipation on the fracture surface, *Phys. Rev. E.* **48,** 439.

Lapusta, N., and J. R. Rice (2003). Nucleation and early seismic propagation of small and large events in a crustal earthquake model, *J. Geophys. Res.* **108,** 2205, doi 10.1029/2001JB000793.

Mai, P. M. (2007). Database of finite-source rupture models, http://www.seismo.ethz.ch/srcmod/ (last accessed February 2008).

Manighetti, I., M. Campillo, S. Bouley, and F. Cotton (2007). Earthquake scaling, fault segmentation, and structural maturity, *Earth Planet. Sci. Lett.* **253,** 429.

Marone, C. J., C. H. Scholz, and R. Bilham (1991). On the mechanisms of earthquake afterslip, *J. Geophys. Res.* **96,** 8441.

Mase, C. W., and L. Smith (1987). Effects of frictional heating on the thermal, hydrologic, and mechanical response of a fault, *J. Geophys. Res.* **92,** 6249.

Pegler, G., and S. Das (1996). Analysis of the relationship between seismic moment and fault length for large crustal strike-slip earthquakes between 1977–1992, *Geophys. Res. Lett.* **23,** 905.

Perfettini, H., and J. Ampuero (2006). Dynamics of a velocity strengthening region and implications for postseismic slip and the generation of slow earthquakes (Abstract T54A-07), *EOS Trans. AGU,* **87** (Fall Meet. Suppl.), T54A-07.

Romanowicz, B. (1992). Strike-slip earthquakes on quasi-vertical transcurrent fault: inferences for general scaling relations, *Geophys. Res. Lett.* **19,** 481.

Romanowicz, B. (1994). Comment on "A reappraisal of large earthquake scaling" by C. Scholz, *Bull. Seismol. Soc. Am.* **84,** 1675–1676.

Schaff, D. P., G. C. Beroza, and B. E. Shaw (1998). Postseismic response of repeating aftershocks, *Geophys. Res. Lett.* **25,** 4549.

Scholz, C. H. (1982). Scaling laws for large earthquakes: consequences for physical models, *Bull. Seismol. Soc. Am.* **72,** 1–14.

Scholz, C. H. (1994). Reply to "Comments on 'A reappraisal of large earthquake scaling' by C. Scholz", *Bull. Seismol. Soc. Am.* **84,** 1677–1678.

Shaw, B. E. (1995). Frictional weakening and slip complexity on earthquake faults, *J. Geophys. Res.* **100,** 18,239.

Shaw, B. E. (1998). Far field radiated energy scaling in elastodynamic earthquake fault models, *Bull. Seismol. Soc. Am.* **88,** 1457–1465.

Shaw, B. E. (2006). Initiation propagation and termination of elastodynamic ruptures associated with segmentation of faults and shaking hazard, *J. Geophys. Res.* **111,** B08302, doi 10.1029/2005JB004093.

Shaw, B. E., and J. R. Rice (2000). Existence of continuum complexity in the elastodynamics of repeated fault ruptures, *J. Geophys. Res.* **105,** 23,791.

Shaw, B. E., and C. H. Scholz (2001). Slip-length scaling in large earthquakes: observations and theory and implications for earthquake physics, *Geophys. Res. Lett.* **28,** 2995.

Sibson, R. H. (1973). Interactions between temperature and pore fluid pressure during earthquake faulting and a mechanism for partial or total stress relief, *Nature Phys. Sci.* **243,** 66.

Thatcher, W., G. Marshall, and M. Lisowski (1997). Resolution of fault slip along the 470-km-long rupture of the great 1906 San Francisco earthquake and its implications, *J. Geophys. Res.* **102,** 5353.

Tsai, V. C., M. Nettles, G. Ekström, and A. M. Dziewonski (2005). Multiple CMT source analysis of the 2004 Sumatra earthquake, *Geophys. Res. Lett.* **32,** L17304, doi 10.1029/2005GL023813.

Tse, S., and J. R. Rice (1986). Crustal earthquake instability in relation to the depth variations of frictional slip properties, *J. Geophys. Res.* **91,** 9452.

Wald, D., and T. Heaton (1994). Spatial and temporal distribution of slip for the 1992 Landers California earthquake, *Bull. Seismol. Soc. Am.* **84,** 668–691.

Wells, D. L., and K. J. Coppersmith (1994). New empirical relationships among magnitude, rupture length, rutpure width, rupture area, and surface displacement, *Bull. Seismol. Soc. Am.* **84,** 974–1002.

Working Group on California Earthquake Probabilities (WGCEP) (2003). Earthquake probabilities in the San Francisco Bay region: 2002 to 2031, *U.S. Geol. Surv. Open-File Rept. 03-214.*

Working Group on California Earthquake Probabilities (WGCEP) (2007). The uniform California earthquake rupture forecast, version 2, *U.S. Geol. Surv. Open-File Rept. 2007-1437.*

Zeng, Y., and J. G. Anderson (1996). A composite source model of the 1994 Northridge earthquake using genetic algorithms, *Bull. Seismol. Soc. Am.* **86,** S71–S83.

Appendix

Model

Model Equations

The bulk equations are a three-dimensional scalar wave equation (mode III elasticity) for the displacement field U:

$$\frac{\partial^2 U}{\partial t^2} = \nabla^2 U, \qquad (A1)$$

where t is time and ∇^2 is the three-dimensional Laplacian operator $\nabla^2 = \partial^2/\partial x^2 + \partial^2/\partial y^2 + \partial^2/\partial z^2$. We use a rectangular geometry, with the fault on a vertical plane, with x the direction along strike of the fault, y the direction perpendicular to the fault, and z the depth direction, down-dip

on the fault. At a far boundary opposite and parallel to the fault, we drive the boundary at a constant slow plate velocity ν, with the boundary condition

$$\left.\frac{\partial U}{\partial t}\right|_{y=L_y} = \nu. \qquad (A2)$$

At the top and bottom of the bulk we have free boundary conditions:

$$\left.\frac{\partial U}{\partial z}\right|_{z=0} = \left.\frac{\partial U}{\partial z}\right|_{z=L_z} = 0. \qquad (A3)$$

Along the fault direction, we use periodic boundary conditions:

$$U(x + L_x) = U(x). \qquad (A4)$$

A viscous boundary layer near the driving boundary damps waves and minimizes reflections. There, the bulk generalizes to

$$\frac{\partial^2 U}{\partial t^2} = \nabla^2 U + \nabla \cdot \xi(y)\nabla\frac{\partial U}{\partial t} \qquad (A5)$$

with $\xi(y) = (y - y_0)\xi_0 \mathcal{H}(y - y_0)$ linearly increasing from zero ($\mathcal{H}$ is the Heaviside step function).

All of the interesting behavior comes from the frictional boundary condition on the fault, which contains all of the nonlinearity in the problem. On the fault, the strain equals the frictional traction stress Φ:

$$\left.\frac{\partial U}{\partial y}\right|_{y=0} = \Phi. \qquad (A6)$$

Friction

We use a stick-slip friction, with a stabilizing viscous term along strike:

$$\Phi = \phi\left(\frac{\partial S}{\partial t'}, t' \leq t\right)\mathbf{H}\left(\frac{\partial S}{\partial t}\right) - \eta\nabla_{\|}^2\frac{\partial S}{\partial t}. \qquad (A7)$$

Here, $\frac{\partial S}{\partial t} = \frac{\partial U}{\partial t}\big|_{y=0}$ is the slip rate on the fault, with ϕ depending on the past history of slip. The function $\mathbf{H}$ is the antisymmetric step function, with

$$\mathbf{H} = \begin{cases} \widehat{\frac{\partial S}{\partial t}} & \frac{\partial S}{\partial t} \neq 0, \\ |\mathbf{H}| < 1 & \frac{\partial S}{\partial t} = 0, \end{cases} \qquad (A8)$$

where $\widehat{\frac{\partial S}{\partial t}}$ is the unit vector in the sliding direction. Thus, $\mathbf{H}$ represents the stick-slip nature of the friction, being multivalued at zero slip rate.

The parameter η is a constant that sets the amount of viscosity and sets the scale at which the small wavelengths are stabilized. The subscript on the viscous term Laplacian denotes that it is the derivative parallel to the fault, which gives $\nabla_{\parallel}^2 = \partial^2/\partial x^2 + \partial^2/\partial z^2$ for the geometry we consider here (Langer and Nakanishi, 1993).

Depth Dependence of Friction

We consider a fault that has two different behaviors: an unstable sliding frictional weakening seismogenic layer from the surface down to a depth H and a stable sliding frictional strengthening layer below that. In the strengthening layer,

$$\phi|_{z>H} = \Phi_0 + a\frac{\partial S}{\partial t}, \qquad (A9)$$

where a is the slope of the velocity-strengthening term. Φ_0 is a constant that sets the sticking threshold. It turns out to be an irrelevant parameter in the problem, as long as it is large compared to the maximum friction drop, so as to prevent backslipping.

In the weakening layer, we use a mixture of slip and velocity weakening, based on a frictional heating mechanism (Shaw, 1995, 1998; Shaw and Rice, 2000):

$$\phi|_{0 \leq z \leq H} = \Phi_0 - \frac{\alpha Q}{1 + \alpha Q}. \qquad (A10)$$

The second term in equation (A10) contains the key dependence on slip and slip rate in the friction, through the variable Q. The variable Q is something like heat, which accumulates with increasing slip rate and dissipates on a timescale $1/\gamma$:

$$\frac{\partial Q}{\partial t} = -\gamma Q + \left|\frac{\partial S}{\partial t}\right|. \qquad (A11)$$

The dissipation with γ gives a simple physically motivated healing mechanism, which also turns out to give a nice range of properties. An equivalent integral solution of Q,

$$Q(t) = \int_{-\infty}^{t} e^{-\gamma(t-t')}\left|\frac{\partial S}{\partial t'}\right| dt', \qquad (A12)$$

shows that, when γ is small compared to unity, the inverse rupture timescale, Q is just the slip in an event, while when $\gamma \gg 1$, Q is $1/\gamma$ times the slip rate. When $\gamma \sim 1$, as we will often use in our three-dimensional simulations, we get a mixture of slip and velocity weakening.

The constant α sets the slope of the stress drop with heat Q. This parameter plays a crucial role in the problem and is a key control parameter.

This heat-weakening friction is a simple mathematical representation (Shaw, 1998) of a physical idea that goes back to Sibson (1973), who considered how frictional heating

raised the temperature and pressure of pore fluids, thereby decreasing the effective normal stress and thus inducing frictional weakening from frictional heating. Shaw (1995) presented simplified self-consistent dynamics of this effect, showing that one got slip weakening and velocity weakening as end-member limits, depending on whether the dissipation of heat was slow or fast, respectively. Earthquakes would be able to dissipate excess pressure with an elastic expansion mode (Mase and Smith, 1987), a mode that can happen on the fast rupture timescale. This fast relaxation mechanism suggests values of γ on the order of unity or larger as the most appropriate values. Thus, a mixture of slip- and velocity-weakening effects are likely occurring. We typically operate in this range because of the physical motivation, but importantly, we also find that, unlike in lower dimensional models where slip weakening alone gives complexity (Shaw, 1995, 1998), in three dimensions we need some velocity weakening as well to get complex sequences of events. If we use slip weakening alone in three dimensions we find, for the parameters we have been able to study, the attracting statistically steady state to be generally system spanning events.

Parameters

A finite difference second-order approximation is made of the bulk equations, which are solved explicitly in time. The default parameter values in the simulations shown are as follows. Geometry parameters $\delta_x = 1/6$, $\delta_z = 1/6$, $\delta_y = 1/12$, $L_x = 80$, and $L_y = 4$; viscous boundary layer parameters $y_0 = L_y - 1$ and $\xi_0 = 0.1$; loading rate $\nu = 0.0003$; and friction parameters $\alpha = 20$, $\gamma = 1$, and $\eta = 0.005$ in the weakening layer and $a = 100$ in the strengthening layer. These parameters are chosen for the following reasons. For the grid resolution parameters δ_x, δ_z, and δ_y, we would like to make these as small as possible, but numerical costs scale as the fourth power of the grid resolution, so we are limited in how small we can make them. We take the grid resolution along the two directions of the fault to be equal. With $\delta_x = \delta_z = 1/6$ we are able to get a range of sizes of small events down to a few kilometers on a side, corresponding to roughly M 5 for real earthquakes. Because we are most interested in very large events, this is sufficient. The grid resolution perpendicular to the fault needs to be even more resolved than the fault parallel direction, and a factor of 2 has been seen to be sufficient for this additional resolution; hence, $\delta_y = 1/12$. Fault parallel domain size L_x needs to be large enough so the longest events generally do not break the whole fault. Periodic boundary conditions are used along the fault. Fault perpendicular domain size L_y should be as large as possible, but numerical costs make this choice, which is large compared to unity, large enough so any imperfectly absorbed waves will not interfere with the dynamics on the fault. A viscous boundary layer away from

the fault is used to damp out waves over a length scale of unity; hence, $y_0 = L_y - 1$, with a linearly increasing viscous term up to a value of $\xi_0 = 0.1$. The friction parameter $\alpha = 20$ is chosen in the range of values where the scaling of small events is consistent with the observed scaling of moment versus area for small events (Hanks, 1977); this occurs over some finite range of α values, a range that appears to increase as grid resolution increases (though we are quite limited in the range of grid resolutions we can explore due to the fourth power dependence of computational time on grid resolution). The parameter $\gamma = 1$ is chosen to get a mixture of slip weakening and velocity weakening. We find we need some velocity weakening to get complex event sequences in three dimensions. The parameter $\epsilon = 0.005$ is chosen to stabilize the small length scales, but not too large that it affects larger scale events. Typical catalog lengths are $\nu t \sim 10$ so that many repeat times of large events are simulated, corresponding to a timescale on the order of thousands of years. The loading rate parameter $\nu = 0.0003$ is chosen as a compromise between wanting small values to have a clear separation of timescales between events but wanting a large value to have a long catalog of events.

Discussion

There is a remarkable insensitivity of the penetration length scale λ to the velocity-strengthening values a: values of $a = 10, 100,$ and 1000 lead to the same effective W. This is additionally significant because we do not use the functional form of velocity strengthening generally expected to hold in the deeper fault, the direct effect of logarithmics velocity-strengthening dependence seen in laboratory measurements (Dieterich, 1979) and inferred from observations (Marone *et al.*, 1991; Schaff *et al.*, 1998). Here, we argue that the insensitivity to this velocity-strengthening parameter supports our use of the numerically simpler linear form. While

we believe this insensitivity to the velocity slope parameter suggests a robustness of our results with respect to treatments of this layer, comparison of our findings with models using more sophisticated deeper rheology would be useful. Tse and Rice (1986) studied two-dimensional quasistatic models with logarithmic velocity strengthening at depth and found only minimal penetration below the seismogenic layer. Lapusta and Rice (2003) studied two-dimensional dynamic models and again found minimal penetration depth. Full rate-and-state equations have additional potential complexities in behavior when the full equations, rather than steady-state approximations, are used (Perfettini and Ampuero, 2006; A. Helmstetter and B. E. Shaw, unpublished manuscript, 2007); thus, the ability of slip to penetrate deeply below the seismogenic layer in a rate-and-state friction framework is an unsettled matter. Indeed, recent work subsequent to this work (Hillers and Wesnousky, 2008) shows quasistatic models with more gradual variations in rate-and-state parameters than used by previous models (Tse and Rice, 1986; Lapusta and Rice, 2003) allow for much deeper penetrating slip. Because some theoretical models clearly allow for it, and the slip-length observations are nicely explained if this is happening, the key question again becomes an observational one: is slip penetrating deep below the seismogenic layer in the Earth?

Lamont-Doherty Earth Observatory
61 Route 9W
Palisades, New York 10964
shaw@ldeo.columbia.edu
(B.E.S.)

Center for Neotectonic Studies
University of Nevada Reno
Reno, Nevada 89557
stevew@seismo.unr.edu
(S.G.W.)